

Multicomponent Synthesis and Binding Mode of Imidazo[1,2-*a*]pyridine-Capped Selective HDAC6 Inhibitors

Marcel K. W. Mackwitz,[†] Alexandra Hamacher,[‡] Jeremy D. Osko,[§] Jana Held,^{||} Andrea Schöler,[†] David W. Christianson,[§] Matthias U. Kassack,[‡] and Finn K. Hansen^{*,†}

[†]Institut für Pharmazie, Universität Leipzig, Brüderstraße 34, 04103 Leipzig, Germany

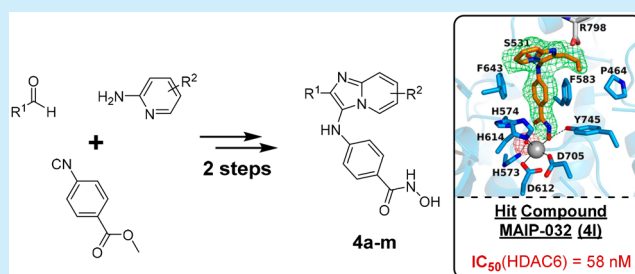
[‡]Institut für Pharmazeutische und Medizinische Chemie, Heinrich-Heine-Universität Düsseldorf, Universitätsstr. 1, 40225 Düsseldorf, Germany

[§]Roy and Diana Vagelos Laboratories, Department of Chemistry, University of Pennsylvania, Philadelphia, Pennsylvania 19104-6323, United States

^{||}Institut für Tropenmedizin, Eberhard Karls Universität Tübingen, Wilhelmstr. 27, 72074 Tübingen, Germany

Supporting Information

ABSTRACT: The multicomponent synthesis of a mini-library of histone deacetylase inhibitors with imidazo[1,2-*a*]pyridine-based cap groups is presented. The biological evaluation led to the discovery of the hit compound MAIP-032 as a selective HDAC6 inhibitor with promising anticancer activity. The X-ray structure of catalytic domain 2 from *Danio rerio* HDAC6 complexed with MAIP-032 revealed a monodentate zinc-binding mode.



The acetylation/deacetylation interplay is a key modification in human cells to control and regulate many important biological processes, such as gene transcription and protein functions.¹ Histone deacetylases (HDACs) play an important role in these posttranslational modifications by cleaving acetyl groups from histone and nonhistone proteins possessing *N*-acetyl-lysine residues.² HDACs are also involved in many diseases such as cancer, neurodegenerative diseases, and inflammation, making these enzymes promising targets for therapeutic approaches.³ Classical HDAC inhibitors (HDACi) can be described by a widely accepted cap-linker-chelator pharmacophore model (Figure 1).^{3b} To date, there are four FDA-approved anticancer HDACi (vorinostat, belinostat, romidepsin, and panobinostat).^{3b} These inhibitors target

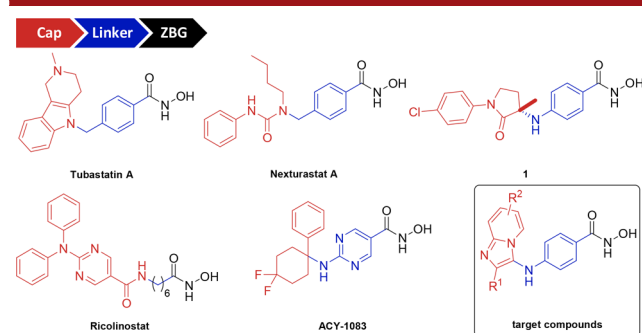


Figure 1. Selected HDAC6 preferential inhibitors and the imidazo[1,2-*a*]pyridine-based target compounds.

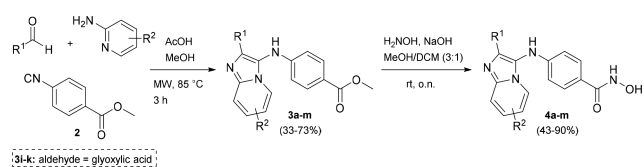
multiple HDAC isoforms, leading to alteration of the acetylation status of many different substrates, which can result in serious unwanted side effects.^{3a,b,e} Therefore, it has been hypothesized that isoform-selective HDACi may enable a more precise regulation and, thus, offer decreased side effects.^{3a,e} HDAC6 modulates the function of many nonhistone proteins, including α -tubulin, Hsp90, cortactin, and many more, thus participating in numerous diseases.⁴ For instance, HDAC6 is highly expressed in several cancer types such as oral squamous cell cancer, advanced stage breast cancer, and acute myeloid leukemia, ensuring migration of cancer cells and angiogenesis.^{3a,4} The knock out of HDAC6 in mice produces a viable phenotype with no significant defects, which may indicate an improved safety profile for HDAC6 selective inhibitors.^{3a} Furthermore, it has recently been reported that HDAC6 differs distinctly in its structural features compared to other isoforms, giving space for bulky rigid cap groups.⁵ In addition, the structural analysis suggests that HDAC6 uses HDAC6-specific loops for the recognition of HDAC6-selective substrates and inhibitors.⁵ Consequently, designing HDAC6i seems to be more approachable compared to other isoforms and several HDAC6 selective inhibitors have been developed (Figure 1).^{4,5} In this context, we report here on the rational design and synthesis of a series of preferential HDAC6 inhibitors containing imidazo[1,2-*a*]pyridine-based cap groups.

Selective HDAC6 inhibitors typically possess a rigid (hetero)cyclic or branched cap group combined with a short benzyl or 4-

Received: April 9, 2018

aminophenyl linker (Figure 1).^{4,5} In this project, we rationally designed bicyclic imidazo[1,2-*a*]pyridine-based hydroxamic acids (Figure 1) and first investigated the potential of these new compounds to inhibit HDAC6 by molecular docking utilizing AutoDock 4.2.⁶ Docking studies were performed in the active site of the catalytic domain 2 of human HDAC6 (PDB ID: SEDU) using an aryl-substituted (**4a**), alkyl-substituted (**4l**), and unsubstituted (**4i**) ligand as representative examples (see Figure S1, Supporting Information (SI)). All three ligands were found to fit smoothly in the active site, and we thus decided to synthesize a mini-library of imidazo[1,2-*a*]pyridine-capped HDACi. The target compounds **4a–m** are accessible by the Groebke–Blackburn–Bienaymé three-component reaction as the key step, followed by hydroxylaminolysis (Scheme 1).⁷ In addition to

Scheme 1. Synthesis of Imidazo[1,2-*a*]pyridine-Based HDACi **4a–m**



the widely commercially available aldehydes and 2-aminopyridines, the isocyanide **2** is required for the synthesis of our target compounds. Thus, we first synthesized isocyanide **2** in a two-step synthesis, starting with the formamidation of methyl 4-aminobenzoate, followed by dehydration (**2**, SI). Subsequently, we optimized the preparative conditions for the Groebke–Blackburn–Bienaymé three-component reaction using intermediate **3a** ($R^1 = 4\text{-Me}_2\text{N-Ph}$; $R^2 = \text{H}$) as model compound. We investigated different catalysts, solvents, temperatures, and reaction times that are described in the literature to identify an efficient procedure for the synthesis of our target compounds.⁷ The best result was achieved by microwave irradiation (150 W) at 85 °C for 3 h with acetic acid as the catalyst and methanol as the solvent with 52% yield for the model compound **3a** (see SI). Furthermore, we were able to synthesize the intermediate **3a** using an isocyanide-less protocol (see SI, 39% yield) adapting the recently published method by Dömling and co-workers.⁸ Due to the slightly higher yield and the efficient access to **2**, we decided to use the classical isocyanide-based protocol for the synthesis of esters **3a–m** (Scheme 1). For the synthesis of the 2-unsubstituted esters **3i–k**, glyoxylic acid was used as a formaldehyde source.^{7c} Pure compounds were obtained either by simple filtration of the crude reaction mixture, if crystallization of the products occurred, or by flash column chromatography in 33–73% yields. Although the possible formation of regioisomers during the Groebke–Blackburn–Bienaymé three-component reaction has been reported, the desired regioselective formation of imidazo[1,2-*a*]pyridines **3a–m** was confirmed for selected compounds through 2D-NOESY-NMR (Figure S2, SI).^{7b} The final step of the synthesis included the hydroxylaminolysis of the esters, which was accomplished in 43–90% yield (**4a–m**) using an excess of aqueous hydroxylamine solution in the presence of sodium hydroxide in methanol/dichloromethane (3:1).

All synthesized hydroxamic acids were evaluated in regards to their inhibitory activity in a biochemical assay against HDAC1 and HDAC6 using ZMAL (Z-Lys(Ac)-AMC)⁹ as a substrate, as previously published (Table 1).¹⁰ First, the HDAC isoform profiling revealed that the majority of compounds showed potent double-digit nanomolar activity against HDAC6. In particular,

Table 1. Activities of **4a–m, Vorinostat, HPOB, and Tubastatin A against HDAC1 and HDAC6**

entry	R ¹	R ²	HDAC1 IC ₅₀ [μM]	HDAC6 IC ₅₀ [μM]	SF ^a
4a		H	0.13(±0.014)	0.050(±0.00035)	3
4b		H	0.89(±0.012)	0.074(±0.0063)	12
4c		H	0.51(±0.057)	0.051(±0.0033)	10
4d		H	0.66(±0.033)	0.12(±0.036)	6
4e		H	0.18(±0.018)	0.14(±0.024)	<2
4f		H	0.17(±0.029)	0.064(±0.0047)	3
4g		H	>3.333	1.33(±0.22)	>3
4h		H	0.27(±0.019)	0.10(±0.0041)	3
4i	H	H	0.84(±0.062)	0.076(±0.0036)	11
4j	H	7-Me	1.01(±0.0035)	0.069(±0.0039)	15
4k	H	6-Me	0.75(±0.043)	0.071(±0.0054)	11
4l		H	2.20(±0.33)	0.058(±0.012)	38
4m		H	1.31(±0.086)	0.057(±0.0034)	23
Vorinostat			0.10(±0.0058)	0.030(±0.0040)	3
HPOB			2.10(±0.23)	0.085(±0.0090)	25
Tubastatin A			2.49(±0.14)	0.014(±0.00061)	178

^aSelectivity factor (SF = IC₅₀ (HDAC1)/IC₅₀ (HDAC6)).

the nature of substituent R¹ seems to be important for the selectivity profile. Aryl-substituted compounds revealed either moderate (**4b–c**; selectivity factor (SF) ≥ 10) or no noteworthy (**4a,e–h**; SF < 10) preference over HDAC1, depending on further substitutions on the phenyl residue. In particular, compounds with a 4-dimethylamino-substituted aryl ring tend to be nonselective inhibitors (see compounds **4a** and **4e**). Compounds **4i–k** with no R¹ substitution displayed moderate preference with selectivity factors of 11–15. Interestingly, compounds **4l** and **4m**, which bear an alkyl group as the R¹ substituent, showed the highest preference over HDAC1. Compound **4l** exhibited the best selectivity factor (SF = 38), comparable to other well-known preferential HDAC6 inhibitors such as HPOB (SF = 25). In order to evaluate its selectivity profile further, **4l** was selected for a screening against the remaining class I isoforms HDAC2, HDAC3, and HDAC8. Strikingly, **4l** was inactive against HDAC2 and HDAC3 (IC₅₀ > 10 μM) and displayed only moderate activity against HDAC8 (IC₅₀: 1.58 ± 0.21 μM; SF^{HDAC8/HDAC6}: 27).

In addition, the preferential inhibition of HDAC6 was studied by Western blotting experiments using the human tongue squamous cell carcinoma cell line Cal27 (Figure S3, SI).

Compounds **4a** and **4l** were selected as representative compounds for aryl and alkyl (R^1) substituted derivatives, whereas the pan-inhibitor vorinostat, the HDAC6 selective HDACi nexturastat, and tubastatin A were used as reference compounds. As expected, vorinostat induced an increase in acetylation of both α -tubulin and histone H3 compared to the control, indicating the inhibition of HDAC6 and class I HDACs. In contrast, compounds **4a**, **4l**, nexturastat, and tubastatin A showed preferential hyperacetylation of α -tubulin. Notably, compound **4l** only induced the acetylation of α -tubulin but not of histone H3, demonstrating that its selective HDAC6 inhibition is retained in a cellular environment.

To investigate the binding mode of **4l**, cocrystallization experiments were performed with the CD2 domain of *Danio rerio* HDAC6 (henceforth, simply "HDAC6"). The 2.50 Å-resolution crystal structure of the HDAC6–**4l** complex (Figure 2) reveals

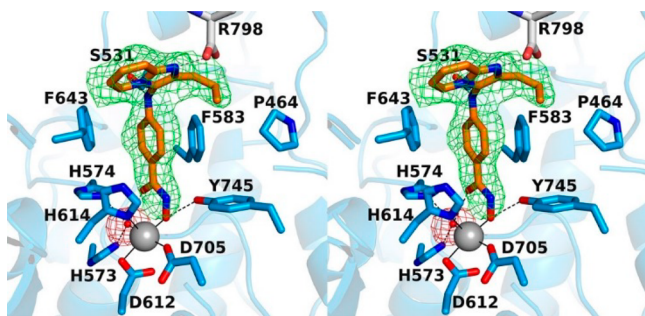


Figure 2. Polder omit maps (stereoview, contoured at 3.0σ each) for **4l** (green) and the Zn^{2+} -bound water molecule (magenta) in the active site of HDAC6. Atom color codes are as follows: C = orange (**4l**) or light blue (protein), N = blue, O = red; Zn^{2+} appears as a gray sphere, and the Zn^{2+} -bound water molecule is shown as a small red sphere. Metal coordination and hydrogen bond interactions are indicated by solid and dashed black lines, respectively.

no major conformational changes between the inhibitor-bound and unliganded states of the enzyme, and the root-mean square deviation is 0.20 Å for 311 $C\alpha$ atoms between the two structures (unliganded HDAC6, PDB accession code 5EEM) (Figure S4, SI). The catalytic Zn^{2+} ion exhibits square pyramidal coordination geometry, with D612, D705, H_2O , and the ionized hydroxamate $N-O^-$ group serving as equatorial ligands and H614 serving as an apical ligand (coordination distance range 2.0–2.4 Å). Several hydrogen bond interactions stabilize the bound inhibitor: the Zn^{2+} -bound hydroxamate $N-O^-$ group accepts a hydrogen bond from Y745, the Zn^{2+} -bound water molecule forms hydrogen bonds with H573 and H574, and the hydroxamate carbonyl group accepts a hydrogen bond from the Zn^{2+} -bound water molecule. Interestingly, the monodentate hydroxamate- Zn^{2+} coordination mode observed for **4l** is also observed for other sterically bulky inhibitors such as HPOB, HPB, and ACY-1083.^{5a,c} The monodentate hydroxamate- Zn^{2+} coordination mode is only 0.5 kcal/mol less stable than the canonical bidentate hydroxamate- Zn^{2+} coordination mode observed for inhibitors with less steric bulk adjacent to the hydroxamate moiety, such as ricolinostat.^{5c} The aromatic ring of the phenylhydroxamate is nestled in an aromatic crevice formed by F583 and F643. The *para*-substituted secondary amino group of **4l** forms a hydrogen bond with S531 on the L2 loop ($N-O$ separation = 3.1 Å).

S531 plays an important role in substrate binding to HDAC6 by accepting a hydrogen bond from the backbone NH group of

substrate acetyl-L-lysine.^{5a} Since S531 is unique to HDAC6, a hydrogen bond with this residue will contribute to HDAC6 inhibitor selectivity. The pendant propyl substituent on the capping group of **4l** is oriented toward P464, and the bicyclic aromatic ring of the capping group is accordingly oriented in the opposite direction toward F643 (Figure 2). Interestingly, aromatic capping groups of many hydroxamate inhibitors are observed to bind adjacent to P464.^{5a,c} However, the region occupied by the bicyclic aromatic ring of **4l** can be exploited further in the design of HDAC6-selective inhibitors, due to the region being occupied by HDAC6 bound substrates. We note that the imidazo nitrogen atom in the heteroaromatic ring of the capping group is presumably protonated, since it is within hydrogen bonding distance to the C-terminal carboxylate of R798 from another HDAC6 molecule in the crystal lattice (Figure 2). Although this interaction is poorly oriented for a hydrogen bond, it could still comprise an electrostatic interaction. Since this interaction could conceivably occur regardless of the orientation of the capping group of **4l**, this interaction is unlikely to significantly influence the binding conformation of **4l**.

To explore the biological activity on a cellular level, all compounds were tested for antiparasitodal as well as anticancer activity (Table S1, SI and Table 2). Besides their promising potency, antiparasitodal HDACi are often disadvantageous as a result of their toxicity against human cells. Therefore, we, and others, hypothesized that selective human HDAC6 inhibitors might be a better starting point for the development of parasite-selective antiparasitodal HDACi due to a usually lower toxicity.^{10,11} Compared to the reference HDACi vorinostat (*Pf*3D7 IC_{50} : 0.209 μM ; *Pf*Dd2 IC_{50} : 0.297 μM), the majority of compounds revealed only moderate activity against the drug sensitive 3D7 (*Pf*3D7 IC_{50} : 0.9–1.9 μM) and the multidrug resistant Dd2 (*Pf*Dd2 IC_{50} : 1.4–6.8 μM) strain. Nonetheless, compounds **4e** (0.524 μM) and **4m** (0.517 μM) showed promising submicromolar antiparasitodal activity against the 3D7 strain.

Next, all synthesized HDACi **4a–m** were assessed in a whole cell HDAC assay using the cell line Cal27 and the class I/IIb selective substrate Boc-Lys(Ac)-AMC (Table 2). All compounds, except **4g** and **4h**, exhibited HDAC inhibition in the whole cell assay, thus confirming the inhibition of cellular histone deacetylase activity. In agreement with the cellular HDAC data, all compounds, except **4g** and **4h**, showed encouraging cytotoxicity in a MTT cytotoxicity assay against Cal27 cells with IC_{50} values ranging from 3.22 to 11.9 μM (Table 2). The highest anticancer activity was observed for compounds **4a**, **4e**, **4j**, **4l**, and **4m** (IC_{50} : 3–4 μM). Flow cytometric analysis using propidium iodide (PI) staining showed that the cytotoxic effect was mediated by induction of apoptosis (Figure S5, SI). Compounds **4a** and **4l** were chosen as representative HDACi. Both compounds increased the amount of apoptotic nuclei in a concentration-dependent manner after 48 h of incubation. Notably, the apoptotic effect was more pronounced for the alkyl substituted HDACi **4l**, even at 1 μM , which is approximately 4-fold below IC_{50} of the MTT assay.

In conclusion, we have developed a multicomponent approach for the synthesis of a mini-library of novel imidazo[1,2-*a*]pyridine-based HDAC6i. Most notably, we show that **4l**, hereafter named MAIP-032, is a selective HDAC6 inhibitor with promising anticancer activity. In addition, the crystal structure of MAIP-032 bound to the second catalytic domain of zebrafish HDAC6 demonstrates a monodentate binding mode. Taken

Table 2. Whole-Cell HDAC Inhibition (HDAC) and Cytotoxic Activity (MTT) against the Human Tongue Squamous Cell Carcinoma Cell Line Cal27 of 4a–m, Vorinostat, Nexturastat A, and Tubastatin A

entry	R ¹	R ²	HDAC (Cal27) IC ₅₀ [μM]	MTT (Cal27) IC ₅₀ [μM]
4a		H	14.0(±1.40)	3.64(±1.24)
4b		H	14.8(±3.14)	4.78(±1.70)
4c		H	13.9(±2.93)	4.53(±1.93)
4d		H	14.0(±1.41)	11.9(±2.72)
4e		H	1.75(±0.27)	3.22(±0.87)
4f		H	14.8(±3.13)	4.60(±1.60)
4g		H	>100	27.7(±8.23)
4h		H	>100	>100
4i	H	H	13.9(±2.93)	4.61(±1.45)
4j	H	7-Me	8.13(±1.08)	3.92(±1.20)
4k	H	6-Me	17.5(±1.85)	4.21(±1.95)
4l		H	27.6(±4.68)	3.87(±1.15)
4m		H	9.38(±3.03)	3.83(±1.40)
Vorinostat			0.87(±0.10)	2.64(±0.10) ^a
Nexturastat A			5.87(±1.70)	7.75(±1.56)
Tubastatin A			11.4(±2.16)	5.34(±0.74)

^aData from refs 4b and 10.

together, the results suggest that MAIP-032 is a promising candidate for further development of selective HDAC6 inhibitors with anticancer properties.

■ ASSOCIATED CONTENT

Supporting Information

The Supporting Information is available free of charge on the ACS Publications website at DOI: 10.1021/acs.orglett.8b01118.

Experimental details (synthetic protocols, bioassays, X-ray crystallography, molecular docking), characterization data of new compounds, and copies of NMR spectra (PDF) HDAC6–4I complex structure (PDB)

Accession Codes

The atomic coordinates and crystallographic structure factors of the HDAC6–4I complex have been deposited in the Protein Data Bank (www.rcsb.org) with accession code 6CGP.

■ AUTHOR INFORMATION

Corresponding Author

*E-mail: finn.hansen@uni-leipzig.de.

ORCID

David W. Christianson: 0000-0002-0194-5212

Finn K. Hansen: 0000-0001-9765-5975

Notes

The authors declare no competing financial interest.

■ ACKNOWLEDGMENTS

We thank Nicholas Porter of the University of Pennsylvania for helpful scientific discussions. Additionally, we thank Tzanko Doukov, Ana Gonzalez, and the beamline 12-2 staff at the Stanford Synchrotron Radiation Lightsource (SSRL), SLAC National Accelerator Laboratory, for assistance with data collection. SLAC is supported by the U.S. Department of Energy (DOE), Office of Science, Office of Basic Energy Sciences under Contract No. DE-AC02-76SF00515. The SSRL Structural Molecular Biology Program is supported by the DOE Office of Biological and Environmental Research, and by the National Institutes of Health, National Institute of General Medical Sciences (Grant P41GM103393). This research was supported by NIH Grant GM49758 to D.W.C. and by the Deutsche Forschungsgemeinschaft (DFG) (HA 7783/1-1 to F.K.H. and HE 7607/1-1 to J.H.).

■ REFERENCES

- (1) Drazic, A.; Myklebust, L. M.; Ree, R.; Arnesen, T. *Biochim. Biophys. Acta, Proteins Proteomics* **2016**, 1864, 1372.
- (2) Biel, M.; Wascholowski, V.; Giannis, A. *Angew. Chem., Int. Ed.* **2005**, 44, 3186.
- (3) (a) Witt, O.; Deubzer, H. E.; Milde, T.; Oehme, I. *Cancer Lett.* **2009**, 277, 8. (b) Mottamal, M.; Zheng, S.; Huang, T. L.; Wang, G. *Molecules* **2015**, 20, 3898. (c) Didonna, A.; Opal, P. *Ann. Clin. Transl. Neurol.* **2015**, 2, 79. (d) Villagra, A.; Sotomayor, E. M.; Seto, E. *Oncogene* **2010**, 29, 157. (e) Su, H.; Altucci, L.; You, Q. *Mol. Cancer Ther.* **2008**, 7, 1007.
- (4) (a) Lin, X.; Chen, W.; Qiu, Z.; Guo, L.; Zhu, W.; Li, W.; Wang, Z.; Zhang, W.; Zhang, Z.; Rong, Y.; Zhang, M.; Yu, L.; Zhong, S.; Zhao, R.; Wu, X.; Wong, J. C.; Tang, G. *J. Med. Chem.* **2015**, 58, 2809. (b) Diedrich, D.; Hamacher, A.; Gertzen, C. G. W.; Alves Avelar, L. A.; Reiss, G. J.; Kurz, T.; Gohlke, H.; Kassack, M. U.; Hansen, F. K. *Chem. Commun.* **2016**, 52, 3219. (c) Shen, S.; Benoy, V.; Bergman, J. A.; Kalin, J. H.; Frojuello, M.; Vistoli, G.; Haeck, W.; Van den Bosch, L.; Kozikowski, A. P. *ACS Chem. Neurosci.* **2016**, 7, 240. (d) Simões-Pires, C. A.; Bertrand, P.; Cuendet, M. *Expert Opin. Ther. Pat.* **2017**, 27, 229.
- (5) (a) Hai, Y.; Christianson, D. W. *Nat. Chem. Biol.* **2016**, 12, 741. (b) Miyake, Y.; Keusch, J. J.; Wang, L.; Saito, M.; Hess, D.; Wang, X.; Melancon, B. J.; Helquist, P.; Gut, H.; Matthias, P. *Nat. Chem. Biol.* **2016**, 12, 748. (c) Porter, N. J.; Mahendran, A.; Breslow, R.; Christianson, D. W. *Proc. Natl. Acad. Sci. U. S. A.* **2017**, 114, 13459.
- (6) Morris, G. M.; Huey, R.; Lindstrom, W.; Sanner, M. F.; Belew, R. K.; Goodsell, D. S.; Olson, A. J. *J. Comput. Chem.* **2009**, 30, 2785.
- (7) (a) Shaaban, S.; Abdel-Wahab, B. F. *Mol. Diversity* **2016**, 20, 233. (b) Buscató, E.; Wisniewska, J. M.; Rödl, C. B.; Brüggerhoff, A.; Kaiser, A.; Rörsch, F.; Kostewicz, E.; Wurglics, M.; Schubert-Zsilavecz, M.; Grösch, S.; Steinhilber, D.; Hofmann, B.; Proschak, E. *Future Med. Chem.* **2013**, 5, 865. (c) Sharma, A.; Li, H. *Synlett* **2011**, 2011, 1407.
- (8) Neochoritis, C. G.; Stotani, S.; Mishra, B.; Dömling, A. *Org. Lett.* **2015**, 17, 2002.
- (9) Heltweg, B.; Dequiedt, F.; Verdin, E.; Jung, M. *Anal. Biochem.* **2003**, 319, 42.
- (10) Stenzel, K.; Chua, M. J.; Duffy, S.; Antonova-Koch, Y.; Meister, S.; Hamacher, A.; Kassack, M. U.; Winzler, E.; Avery, V. M.; Kurz, T.; Andrews, K. T.; Hansen, F. K. *ChemMedChem* **2017**, 12, 1627.
- (11) De Vreese, R.; de Kock, D.; Smith, P. J.; Chibale, K.; D'hooghe, M. *Future Med. Chem.* **2017**, 9, 357.